Nonequilibrium study of the forces responsible for adsorption in a binary liquid mixture

Dean Ripple* and Carl Franck

Laboratory of Atomic and Solid State Physics and Materials Science Center, Cornell University, Ithaca, New York 14853

A new nonequilibrium technique is used to investigate the intermolecular forces that determine the thickness of wetting layers in the system methylcyclohexane plus perfluoromethylcyclohexane on silicon near the critical point of the liquids. When the liquids are subjected to a linear temperature ramp, the resulting deviation from equilibrium controls the thickness of the methylcyclohexane-rich wetting layer. Ellipsometric measurements of the layer thickness for thermodynamic states corresponding to temperatures 0.5 to 50 mK above the coexistence curve agree quantitatively with theoretical calculations. As the distance from coexistence decreases, the layer thickness smoothly increases and shows a crossover from adsorption dominated by the nonzero correlation length to adsorption dominated by dispersion forces. The measurements also confirm that correlations in the concentration decay exponentially, out to at least five correlation lengths. Equilibrium measurements on an off-critical concentration cell in the single-phase region agree with theory for temperatures greater than 0.2 K from the coexistence curve, but show marked irreproducibility within 0.2 K of the transition.

I. INTRODUCTION

When a substrate, which preferentially adsorbs A molecules over B molecules with sufficient strength, is immersed in a binary liquid mixture rich in B molecules, the amount of A-rich adsorption depends on the detailed nature of the intermolecular forces and on the relative free energies of the bulk and adsorbed liquid. Dispersion forces [1,2], electrostatic forces [3,4], capillary waves [5], and the proximity of the liquid-liquid critical point [6] may all contribute to the adsorption. Along the coexistence curve, bulk A-rich and B-rich phases are both allowed, and the substrate will be wet by a macroscopically thick layer of A-rich liquid. Moving away from coexistence into the single-phase B-rich region, A-rich liquid will be thermodynamically metastable, and the adsorption will drop. The distance in temperature or concentration from coexistence determines the free-energy difference between the adsorbed and bulk liquids, so simultaneous measurement of the adsorption and variation of the distance from coexistence characterizes the forces over a tunable range of free energy. In this paper we describe a nonequilibrium means of controlling the distance from coexistence, and with the aid of this technique we determine the intermolecular forces responsible for adsorption in near-critical mixtures of methylcyclohexane (labeled MC, formula C_7H_{14}) plus perfluoromethylcyclohexane (labeled PFMC, formula C_7F_{14}) on an oxide-coated silicon wafer. Experiments on the nonequilibrium technique itself clarify how a two-phase liquid system relaxes to equilibrium, independent of any surface adsorption.

We control by two separate means the distance from coexistence. With the liquid in the single-phase region and at equilibrium, we vary the temperature from slightly above the bulk transition temperature T^* up to several degrees above T^*. With the liquid in the two-phase re-

gion, we drive the liquids out of equilibrium and off coexistence by linearly ramping the temperature of the liquid mixture while continuously stirring. The equilibrium method has been documented elsewhere [3,7], but the nonequilibrium method is newly developed and described fully in this paper. In steady state the rate at which the temperature ramp pushes the system off coexistence balances the relaxation of the volume fraction of A, ϕ, back to its equilibrium value. Variations in ramp rate or in stir rate, which determine the relaxation rate, tune the deviation from coexistence. We use null ellipsometry to measure the optical reflection properties of the liquid–adsorbed-layer–substrate interface, and by optically modeling the solid and liquid media we then find the adsorption at the surface.

Experimental difficulties in locating the bulk transition temperature to better than a few millikelvin limit the precision of the equilibrium method. Using gravity to thin adsorbed layers theoretically probes states much closer to coexistence [8], but the diffusion time necessary for equilibrium over centimeter size cells can easily exceed several weeks [8,9], and convection caused by very small horizontal temperature gradients may strongly disturb the gravitational sedimentation [10,11]. Advantages of the temperature ramp technique over either of these equilibrium techniques include approach to within 0.5 mK of coexistence with complete insensitivity to convection, equilibration times of a few hours, and a dynamic range of 2–3 orders of magnitude in deviation from coexistence.

We have compared nonequilibrium measurements with equilibrium measurements from the same sample cell as well as with theoretical predictions for the adsorption. We find that the equilibrium data for temperatures more than 0.2 K above coexistence and all of the nonequilibrium data are reproducible and agree with theoretical estimates of the adsorption. Our measurements confirm that

the dispersion force theory of Dzyaloshinskii, Lifshitz, and Pitaevskii [1] (DLP for short) works well for binary liquid mixtures and that the simple, phenomenological model of Widom [6] correctly describes forces on the wetting layer caused by the proximity of the critical point, but we see no strong contribution to the adsorption by either capillary waves [5] or power-law correlations in the concentration of the liquids [2,12,13]. As expected for nonpolar liquids, we detect no contribution of electrostatic forces in this binary liquid system.

As further evidence that we understand the nonequilibrium processes in the ramp technique, the change in ϕ following a change in temperature ramp rate obeys the exponential decay law predicted by the theory for mass transport between the two coexisting liquid phases and the wetting layer, and the decay has a time constant consistent with hydrodynamic estimates.

Within 0.2 K of the bulk transition temperature, the amount of adsorption determined by equilibrium measurements in the single-phase region significantly exceeds both the theoretical predictions and the ramp-technique results. This difference may be related to hysteresis and irreproducibility from cell to cell observed for temperatures within 0.2 K of T^* as well as difficulty in locating T^* accurately.

A previous investigation [14] studying the effects of temperature modulations on wetting layers gave results in qualitative agreement with theoretical predictions, but a variety of difficulties prevent a quantitative comparison. The variation of temperature with time may cause both thermal gradients and convection, resulting in an unpredictable transport of fluid through the cell. Furthermore, the initial thermodynamic state about which the temperature varies is subject to the same uncertainties as experiments on gravity-thinned wetting layers. In the temperature ramp experiments presented here, forced convection dominates any thermally induced convection, the thermal gradients are small, and the thermodynamic state of the bulk fluid is well known. As a consequence of these improvements, we can make quantitative comparisons between the experimental results and both the theory of material transport and the theory of equilibrium adsorption.

Because interpretation of the data relies on a few theoretical results of thermodynamics and hydrodynamics that are independent of the theory for the adsorption, we organize the remainder of the paper into the following sections: Sec. II describes the equipment and technical details of the experiment, Sec. III outlines the theory of the equilibrium and nonequilibrium techniques, Sec. IV presents the theory of adsorption, Sec. V gives experimental observations, and finally, we present conclusions in Sec. VI.

II. EXPERIMENTAL DETAILS

The sample cell design [15] consists of a silicon wafer suspended vertically along the axis of a test-tube-shaped glass cell and immersed in the binary liquid mixture. A spring or clamp holds the wafer against a stainless-steel plate, which in turn seals against the glass cell walls with
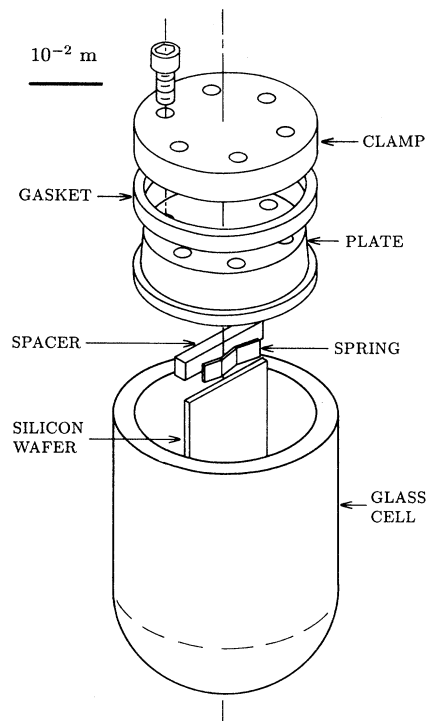
FIG. 1. Sample cell design. To seal the cell, the clamp at the top of the cell compresses a Teflon gasket between the plate and the cell wall. The silicon wafer, spring, and spacer fit into a slot milled in the bottom of the plate. The liquids and stir bar held by the cell are not shown, and some details of the stainless-steel plate have been omitted for clarity.

either a Teflon or Viton gasket. A Teflon-coated magnetic stir bar rests at the rounded bottom of the cell and can be rotated at speeds ranging from 0.6 to 5 Hz by the field of a large rotating magnet situated outside the thermostat. Figure 1 shows an exploded view of the cell design.

The geometry of the cell allows us to reflect an incident He-Ne laser beam, lying in a horizontal plane, off of the silicon surface at any incident angle and at any vertical position along the wafer. For the experiments done with two coexisting liquid phases, the laser passes through the lower liquid phase, rich in PFMC. The cylindrical cell design acts as a lens on the incident beam, and consequently displacement of the silicon surface from the optical axis by a few tenths of a millimeter results in a shift of the incident angle by a few tenths of a degree, a definite disadvantage of this cell design. To correct for this beam steering and for uncertainties in the refractive indices of the silicon and the bulk liquid phase, we reference the ellipsometer angle off of the measured Brewster's angle. That is, we compare the measured angle at which the reflectivity of P-polarized light drops to a minimum with the angle predicted by our optical modeling, and we use the difference as a correction to the ellipsometer angle scale.

The cell rests in a four stage thermostat [15], constructed of concentric metal shells thermally isolated from one another. The outer three shells, labeled stages 1, 2, and 3, with stage 1 outermost, are actively temperature regulated with integrating controllers. To reduce thermal gradients, the sample cell mounts inside a fourth passive metal shell, stage 4. All of the metal shells have apertures allowing passage of the laser beam for incident angles of 65° to 77°, in the vicinity of Brewster's angle. To minimize heat loss caused by convection, annealed glass windows cover the stage-3 apertures. Stages 3 and 4 mount to a six degree of freedom tilt and translation stage inside stage 2, so the inner two thermostat stages move as a unit when adjusting the optical alignment of the ellipsometer.

Thermal stability of the thermostat is approximately 50 μK over an hour and 100 μK over a day, as measured by a bridge circuit and thermistors independent of the temperature controller. Measurements with copper-constantan thermocouple pairs give an upper limit for thermal gradients in the sample cell of 60 μK cm^{-1}. For each thermocouple pair we made a measurement, reversed the mounting position of the two thermocouple junctions, and then repeated the measurement in order to make a differential measurement of the thermal gradient independent of any spurious voltage sources in the lead wires. Measurements with a more sensitive thermistor pair indicated that stirring at 5 Hz contributes additional gradients of less than 10 μK cm^{-1} and ramping the temperature at 24 mK h^{-1} contributes a gradient of 0.2 mK cm^{-1}. At these low gradients and with an absorbing substrate such as silicon, the incident laser power must be reduced to as low as 10^{-7} W to avoid laser heating results.

By connecting a stepping motor to the set point knob of the stage-3 temperature controller and driving the motor with pulses from a digital clock, we can impose temperature ramps on the thermostat which are linear and accurate to 50 μK h^{-1}.

We use null ellipsometry [16,17] to measure the two ellipsometric parameters, δ and ψ, which characterize the ratio and phase shift of the reflection coefficients, r_S and r_P, for S and P polarized light:

$$r_S = |r_S| e^{i\delta_S}, \quad r_P = |r_P| e^{i\delta_P} ; \qquad (1)$$

$$\delta = \delta_S - \delta_P, \quad \tan\psi = \frac{|r_P|}{|r_S|} . \qquad (2)$$

Note that the standard notation for δ is Δ, but Δ refers to a free-energy amplitude in Sec. IV. Polaroid sheet and a prism polarizer serve as the polarizer and analyzer, respectively, although we observe no changes in the data when we use prism polarizers for both components. The compensator is a sheet of bare mica, and we fix its fast axis at 45° from the horizontal, measuring the angle counterclockwise while facing the light source. Because the curved cell walls act as a defocusing lens on the incident beam, we insert an aperture behind the analyzer to select a range of ±0.3° in exit angle. Even at the low light levels needed to avoid heating, a photodiode detector optimized for minimal noise has sufficient sensitivity,

provided that we chop the incident light at a few hundred hertz and feed the photodiode signal to a lock-in amplifier.

We prepared two separate cells, numbers 1 and 2, using identical liquids and substrates, but with somewhat different cell sealing methods and filling techniques. Cell 1 had a Viton O ring as a seal for the stainless-steel plate, and a small stainless-steel wedge and screw clamped the silicon wafer into position. Because of some anomalous results obtained with cell 1, as described in Sec. V, we sought to seal cell 2 with a more inert gasket and to avoid any hard-to-clean screw threads, which could also trap a dead volume of liquid. Cell 2 consequently relied on a stainless-steel spring to hold the silicon and a compressed Teflon gasket to seal the cell.

In both cases, we followed identical cleaning procedures. Glass was cleaned with warm (≈ 60 °C) detergent solution, ethylenediamine tetra-acetic acid (EDTA) solution, 10% nitric acid, with extensive distilled water rinses between solutions and as a final rinse. Similarly, Teflon was cleaned with detergent solution and hydrogen peroxide, stainless steel with detergent solution and nitric acid, and Viton with detergent, again all with water rinses. After a final rinse with distilled water that had been filtered to remove particles larger than 0.5 μm all of these parts were vacuum baked at 70 °C for 3 h. The silicon wafer was cleaned by organic strippers recommended for metal-oxide-semiconductor field-effect transistor (MOSFET) substrates [18]: soaking in a warm mixture of 97% sulfuric acid and 31% hydrogen peroxide (4:1 by volume), followed by a water rinse and then soaking in a warm 29% ammonium hydroxide, hydrogen peroxide, and water mixture (1:1:5 by volume). Many water rinses followed, and to avoid contamination from the air, the wafer was stored in water until just prior to cell assembly.

Assembly of the cell began by blowing the silicon dry with filtered argon gas and mounting the silicon onto the top plate. After transferring the cell parts to a glove bag and purging with argon, we filled the cells with $\phi_T = 0.338 \pm 0.006$ total volume fraction of MC. (Throughout this paper, quoted errors correspond to a 2 σ or 90% confidence level uncertainty, unless stated otherwise.) The MC and PFMC were used without further purification [19], but for cell 2, we filtered the liquids with a 0.5-μm filter. Shortly after filling, cell 1 had a transition temperature $T^* \approx 43.3$ °C, and cell 2 had $T^* \approx 43.0$ °C. The data of Heady and Cahn [20], for comparison, give

$$T^* \approx 43.4 \, °\text{C} .$$

III. THEORY OF MEASUREMENTS

We take the equilibrium data in the single-phase region, along a trajectory of constant volume fraction of MC $\phi = \phi_T$ and at temperatures above T^*. Theoretically, at temperatures close enough to T^* gravitational sedimentation will cause spatial variations in ϕ [9], and the exact thermodynamic trajectory will depend on possible convection of the liquid and the vertical height of the substrate being probed. In practice the experimental uncertainty in T^* limits the experiments to states much far-
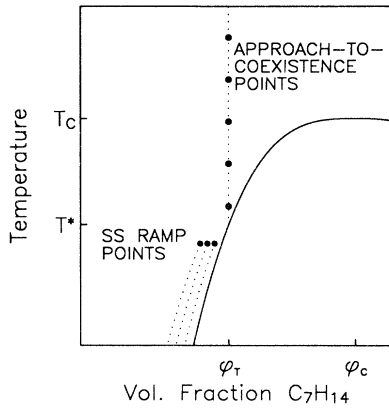
FIG. 2. Thermodynamic trajectories. All equilibrium data lie along a line of fixed total concentration $\phi_T = 0.338$ and at a temperature above the bulk transition temperature T^*. Steady-state nonequilibrium data lie along a line of fixed temperature below T^*, but the temperature rises continuously before and during the measurement.

ther from coexistence than the gravity-dominated regime [7,21]. Gentle stirring, weak enough to not hydrodynamically disturb the adsorbed layer, should have a minimal effect on the quantity of adsorption, since the temperature field and not any spatial variation of ϕ determines the deviation from coexistence. As shown in Fig. 2, we label the equilibrium, single-phase trajectory "approach to coexistence."

The nonequilibrium trajectories, also illustrated in Fig. 2, rely on the finite relaxation time of a binary liquid mixture towards equilibrium when the temperature is disturbed. Imagine that the mixture initially is in full thermodynamic equilibrium and in the two-phase region. We will label the upper liquid phase, rich in MC, by M and the lower phase, rich in PFMC, by P. If the temperature increases, diffusive transport will bring the mixture into equilibrium only within a distance $l \approx (\tau D)^{1/2}$ from the liquid-liquid meniscus after time τ and with diffusion constant D. Without stirring, equilibration of the bulk liquid phases by diffusion would take weeks for the 1-cm distances characteristic of the sample cell [8]. With stirring, convection will transport material through most of the bulk phase much more efficiently than diffusion, but near the phase boundaries hydrodynamics limits the mass transport. Near the liquid-liquid meniscus, when stirring is gentle, convection can only transport fluid parallel to the meniscus. Within a diffusion boundary layer, of characteristic thickness l_{DBL}, diffusion must be the dominant transport process across the meniscus [8]. Because we study the adsorption of M phase with the heavier P phase as the bulk liquid, we now focus on the dynamics of the mixture below the liquid-liquid meniscus. We assume diffusion across the meniscus fixes the volume fraction a microscopic distance below the meniscus to the equilibrium, coexistence value at the current temperature, ϕ_{co}. When the volume fraction outside the boundary layer, ϕ, deviates from ϕ_{co}, a gradient $\nabla \phi = (\phi - \phi_{\mathrm{co}})/l_{\mathrm{DBL}}$ is established across the boundary layer, and the flux through this layer is [22]

$$ J = -D \left[\frac{\phi - \phi_{\mathrm{co}}}{l_{\mathrm{DBL}}} \right] . \tag{3}$$

Because the experimental measurements depend most directly on J and $\phi - \phi_{\mathrm{co}}$, it is convenient to take this flux equation, Eq. (3), as a definition of l_{DBL} rather than define l_{DBL} hydrodynamically, as in Ref. [8]. Integrating the flux over the whole meniscus area, and defining an average diffusion boundary layer thickness as

$$ \frac{1}{L_{\mathrm{DBL}}} \equiv \frac{1}{A} \int dA \frac{1}{l_{\mathrm{DBL}}} \tag{4}$$

we get the total volume fraction current

$$ JA = -\frac{DA}{L_{\mathrm{DBL}}}(\phi - \phi_{\mathrm{co}}) , \tag{5}$$

where A is the cross-sectional area of the meniscus. The ratio of this current to the volume of the liquid phase, V, determines the rate at which the bulk value of ϕ relaxes to equilibrium. Mathematically, with $L \equiv V/A$ being the effective height of the phase and τ being time,

$$ \frac{\partial \phi}{\partial \tau} = -\frac{D}{L L_{\mathrm{DBL}}}(\phi - \phi_{\mathrm{co}}) . \tag{6}$$

We define a characteristic time $\tau_0 \equiv L L_{\mathrm{DBL}}/D$ and rewrite Eq. (6) in terms of the new variable $\tilde{\phi} \equiv \phi - \phi_{\mathrm{co}}$ to get

$$ \frac{\partial \tilde{\phi}}{\partial \tau} = -\frac{\tilde{\phi}}{\tau_0} - \frac{d\phi_{\mathrm{co}}}{d\tau} . \tag{7}$$

Allowing the temperature to vary at a rate $\dot{T}$, we obtain the general equation for the difference between ϕ and the equilibrium volume fraction in the temperature ramp experiments:

$$ \frac{\partial \tilde{\phi}}{\partial \tau} = -\frac{\tilde{\phi}}{\tau_0} - \left[\frac{d\phi_{\mathrm{co}}}{dT} \right] \dot{T} . \tag{8}$$

All of the experimental measurements satisfy the conditions $\tau_0 \dot{T} \ll (T_c - T)$ and $\dot{T} = $ const, and the solution to Eq. 8 is by inspection

$$ \tilde{\phi} = A e^{-\tau/\tau_0} - \tau_0 \dot{T} \left[\frac{d\phi_{\mathrm{co}}}{dT} \right] , \tag{9}$$

where $(d\phi_{\mathrm{co}}/dT)$ is assumed to be constant.

In the steady state limit, the deviation from coexistence varies linearly with both temperature ramp rate and τ_0 and can be expressed in terms of a shift of either volume fraction or temperature away from coexistence:

$$ \tilde{\phi}_{\mathrm{SS}} = \phi_{\mathrm{SS}} - \phi_{\mathrm{co}} = -\tau_0 \dot{T} \left[\frac{d\phi_{\mathrm{co}}}{dT} \right] , \tag{10}$$

$$ T - T_{\mathrm{co}} = -\tau_0 \dot{T} , \tag{11}$$

where T_{co} is the temperature at which ϕ_{SS} is at two-phase coexistence.

In principle, τ_0 could be determined by calculating the hydrodynamic flows in the cell, but the complicated cell geometry precludes anything but an estimate of τ_0. A

very simple approximation replaces the cell volume by a cylindrical cavity, replaces the stirrer by a rotating bottom plate, and neglects any flow of the liquid-liquid meniscus. The diffusion boundary layer in this case does not vary in thickness over the meniscus and to within a factor of order one has thickness [8]

$$L_{DBL}(\text{estimate}) = \left[\frac{D}{v} \right]^{1/3} \left[\frac{v}{2\pi f} \right]^{1/2} , \quad (12)$$

where v is the kinematic viscosity of the stirred phase and f the stirring frequency. For a geometry close to the actual cell geometry, a stir rate of 1 Hz, and a temperature 3 K below the critical temperature, Eq. (12) gives $L_{DBL}(\text{estimate}) = 1.7 \times 10^{-5}$ m, which implies $\tau_0(\text{estimate}) = 0.75$ h.

To know $\tilde{\phi}$ or $T - T_{co}$ in absolute units, we must measure τ_0. For concreteness, we describe how τ_0 can be determined from the measurements of δ, but an equivalent analysis applies for ψ measurements. The steady state ramp data consist of a set of data pairs $(\delta, \dot{T})$, which we parametrize as $\delta = g(\dot{T})$. Inversion of the function g and substitution into the steady state solution for $\tilde{\phi}$ results in a relation between δ and $\tilde{\phi}$:

$$\tilde{\phi} = -\tau_0 \dot{T} \left[\frac{d\phi_{co}}{dT} \right] = -\tau_0 g^{-1}(\delta) \left[\frac{d\phi_{co}}{dT} \right] . \quad (13)$$

If we change the temperature ramp discontinuously, the general solution for $\tilde{\phi}$, Eq. (9), predicts an exponential relaxation of $\tilde{\phi}$ to its new steady state value,

$$\ln \left[\frac{|\tilde{\phi} - \tilde{\phi}_{SS}|}{\tau_0} \right] = - \left[\frac{1}{\tau_0} \right] \tau + (\ln|A| - \ln\tau_0) . \quad (14)$$

We measure the relaxation of δ with time, and with the above map, Eq. (13), the values of δ measured during the relaxation are converted into $\tilde{\phi}/\tau_0$. By Eq. (14), a plot of $\ln(|\tilde{\phi} - \tilde{\phi}_{SS}|/\tau_0)$ versus τ should then be linear with a slope $-1/\tau_0$.

The above theory describes the thermodynamic state at which we take each measurement. We also need a set of optical models to convert the ellipsometry data into a measure of the quantity of adsorption. Near coexistence, the volume fraction of the adsorbed liquid is uniform over most of its thickness, and we can refer to a "wetting layer" of volume fraction ϕ_{WL} and thickness l. Far from coexistence, the adsorbed layer is little thicker than the bulk correlation length, and a better measure of the amount of MC attracted to the surface is the adsorption Γ, equal to the zeroth moment of the profile:

$$\Gamma = \int_0^\infty dz [\phi(z) - \phi_B] , \quad (15)$$

where $\phi(z)$ gives the average volume fraction of MC as a function of distance z from the wall, and ϕ_B is the volume fraction of the bulk liquid. For our experimental arrangement, the z axis lies in the horizontal plane, normal to the silicon surface. In the limit $T \rightarrow T_{co}$ the bulk liquid and wetting layer have volume fractions ϕ_B and ϕ_{WL}, and we can normalize the adsorption Γ to get $\Gamma/(\phi_{WL} - \phi_B)$, which for states close to coexistence

equals the wetting layer thickness plus a small positive constant resulting from the sharp increase in ϕ near $z = 0$.

Rather than assume a slab profile of the refractive index through the wetting layer, we use the more realistic profiles of Sec. IV to obtain $\phi(z)$. To convert the $\phi(z)$ profile into a refractive index profile, we use literature values for the refractive indices of the pure components [23,24] plus the Lorentz-Lorenz relation [25]. Assuming that there is no significant change in volume upon mixing and that the only temperature dependence results from the change in density with temperature, the Lorentz-Lorenz relation gives

$$f(n^2) = \phi \frac{\rho_{MC}(T)}{\rho_{MC}(20°C)} f([n_{MC}(20°C)]^2)$$

$$+ (1-\phi) \frac{\rho_{PFMC}(T)}{\rho_{PFMC}(20°C)} f([n_{PFMC}(20°C)]^2) , \quad (16)$$

$$f(n^2) \equiv \frac{n^2 - 1}{n^2 + 1} . \quad (17)$$

We use the density functions given by Heady and Cahn, [20], and pure refractive indices for the laser wavelength of 633 nm of $n_{MC}^2(20°C) = 2.0207$ and $n_{PFMC}^2(20°C) = 1.6427$.

From literature values [26,27], the refractive index of the bulk silicon and the oxide overlayer are $3.867 + 0.020i$ and 1.460. Ellipsometric measurements of silicon wafers in air imply the existence of a transition layer between the oxide and the pure silicon [26]. Converting the results of Aspnes and Theeten [27] to a 633-nm wavelength, the transition layer has an apparent thickness of 0.7 ± 0.2 nm (1 σ error) and a refractive index of 3.2 ± 0.5 (1 σ). The optical modeling of dielectric media used to interpret the ellipsometric results will break down for layer thicknesses of a few molecular spacings or less [3,28], so it is not clear whether the 0.7-nm layer corresponds to a true transition layer or merely compensates for the nonlocality of the dielectric response near a sharp silicon-silicon dioxide interface.

Unfortunately, we have found that the interpretation of the ellipsometric data depends on the choice of parameters for this transition layer. We made two measurements of the oxide layer thickness, d_O, for the cell 2 silicon wafer, once in air and once with the wetting phase adjacent to the substrate. In both cases there is no thick wetting layer, and we can determine the thickness of the oxide layer from the ellipsometric parameters, given any assumed transition layer model. We vary the transition layer thickness d_T and refractive index n_T independently by approximately 1 σ errors to test the dependence of $\Gamma/(\phi_{WL} - \phi_B)$ on the choice of transition layer model. We found that the oxide thickness determined by the in-air and in-liquid measurements agreed within experimental errors for the transition layer models ($n_T = 2.6$, $d_T = 0.5$nm), (3.2, 0.7 nm), and (3.6, 0.9 nm), but disagreed for the models (3.6, 0.5 nm) and (2.6, 0.9 nm) and a model with no transition layer at all. For the data analysis we choose the model (3.2, 0.7 nm) for the transition layer. Errors in the ellipsometric measurements used to determine d_O and uncertainties in the exact transition

layer parameters result in systematic errors of a few nanometers in the quantity $\Gamma/(\phi_{WL}-\phi_B)$. We quantify the errors in Sec. V.

With the complete refractive index profile specified, we calculate the parameters δ and ψ for any adsorption profile by a matrix method [28], and by fitting the theoretical $\Gamma/(\phi_{WL}-\phi_B)$ versus δ or ψ results to a polynomial, we obtain a mapping of experimental ellipsometry results to adsorption. The maps used to convert the raw data into the symbols in the figures are given in Appendix A.

IV. THEORY OF ADSORPTION

A simple postulate for calculating the adsorption of a near-critical liquid mixture of A and B molecules at a surface is to assume that a short-range force perturbs ϕ at the surface, resulting in a profile $\phi(z)$ decaying away from the wall towards the bulk value ϕ_B. Far above T_{co}, but within a few kelvin of the critical temperature, and at length scales large compared to the intermolecular spacing, ϕ will decay exponentially with a characteristic length ξ, the bulk correlation length [6,29,30]. In contrast, if the surface favors A molecules and the bulk liquid is more B-rich than the critical concentration, then $\phi(z)$ will have a slablike profile for small $T-T_{co}$ [31]. The profile will have a plateau at a value of ϕ close to the concentration of the A-rich phase at coexistence, and this plateau is termed a "wetting layer."

Close to coexistence, the free energy of the interface can be written as a function of the single parameter l, the wetting layer thickness. Our approach-to-coexistence data extend up to 3 K above T^*, though, and a slablike wetting layer poorly approximates the actual adsorption profile. To avoid the restriction of an assumed adsorption profile, we write the interfacial grand potential Ω as a functional of $\phi(z)$ [30]:

$$\Omega = \int_0^\infty dz \left[\tfrac{1}{2} m(\phi')^2 + f_e(\phi,\phi_B,t) \right] \qquad (18)$$

where f_e is the excess free energy per unit volume to create liquid of volume fraction ϕ out of liquid of volume fraction ϕ_B at reduced temperature $t=(T-T_c)/T_c$, and m is a coefficient that varies only slowly with temperature. We assume that ϕ at the substrate has a fixed value ϕ_s, and then the Euler equation which minimizes Ω is

$$m\phi'' = \left[\frac{\partial f_e}{\partial \phi} \right]_{t,\phi_B} . \qquad (19)$$

For all of the calculations we assume $\phi_s = 1$, corresponding to pure MC at the substrate (as is done by Liu and Fisher in Ref. [6]).

A previous paper [3] demonstrates how to determine f_e from a universal scaling function and how two-scale universality determines all of the relevant thermodynamic parameters given experimental amplitudes of only two critically diverging quantities. Heady and Cahn [20] actually measured three critical amplitudes for the system PFMC and MC: surface tension, the coexistence curve, and the curvature of the free energy, which is proportional to f_e. Although the experimental evidence for two-scale factor universality is strong [32], the amplitude of

f_e from the free-energy data exceeds by a factor of 3–4 the amplitude found using two-scale factor universality and data for the coexistence curve and surface tension. Because the surface tension data agree to within 20% of a previous measurement [33] in the temperature range of our data and because the coexistence curve measurement is both simple and reliable, we are most skeptical of the free-energy data. These data also imply that near T_c but in the single-phase region, $f_e < 0$, an unphysical result. For these reasons, we find the necessary amplitudes from only the coexistence curve and surface tension measurements, plus scaling theory and amplitude ratios.

Because the published results of Heady and Cahn do not use accepted renormalization-group values for the critical exponents [30], we have shifted the surface tension exponent and refit the coexistence curve. For the surface tension, we find $\sigma = \sigma_0 |t|^\mu$, with $\sigma_0 = 2.27 \times 10^{-2}$ J m^{-2} and $\mu = 1.26$. We assume a functional form for the coexistence curve of

$$\tfrac{1}{2}(\phi_M + \phi_P) = \phi_c + C|t| , \qquad (20)$$

$$\phi_M - \phi_P = B|t|^\beta + B_1|t|^{\beta+\Delta_2} , \qquad (21)$$

and with fixed $\beta = 0.325$ and $\Delta_2 = 0.5$, find for the amplitudes $\phi_c = 0.5403$, $C = -0.280$, $B = 1.951$, and $B_1 = -0.694$. This parametization has an estimated accuracy of 6×10^{-4} in ϕ for the range of t needed for the experiments described in this paper.

We refer to Ref. [3] for a detailed discussion of the appropriate amplitude ratios and notation, and we give here only the final results. For the coefficient of the gradient term, we find $m = m_0 |t|^{-\eta\nu}$, with $\eta\nu = 0.02$ and $m_0 = 4.84 \times 10^{-12}$ J m^{-1}. For the derivative of the excess free energy we find

$$\left[\frac{\partial f_e}{\partial \phi} \right]_{t,\phi_B} = \Delta(\phi,t) - \Delta(\phi_B,t) , \qquad (22)$$

where the deviation of Δ from its value along the coexistence curve, Δ_c, is given in terms of a scaling function [34] $h(x)$:

$$\Delta - \Delta_c = \Delta_c \left[\frac{\phi - \phi_c}{\phi_c} \right] \left| \frac{\phi - \phi_c}{\phi_c} \right|^{\delta-1} h(x) , \qquad (23)$$

$$h(x) = E_1 \left[\frac{x}{x_0} + 1 \right] \left[1 + E_2 \left[\frac{x}{x_0} + 1 \right]^{2\beta} \right]^{(\gamma-1)/2\beta} , \qquad (24)$$

$$x \equiv t \left| \frac{\phi - \phi_c}{\phi_c} \right|^{-1/\beta} . \qquad (25)$$

Renormalization-group calculations give for the exponents $\gamma = 1.24$ and $\delta = 4.81$ [30,35]. The necessary amplitudes [3,20,30,32,35] for PFMC plus MC are $E_1\Delta_c = (6.2\pm1.9)\times10^6$ J m^{-3}, $E_2 = 0.30\pm0.02$, and $x_0 = 0.1912\pm0.0057$.

We solve the Euler equation numerically, and from each profile we find the wetting layer thickness, equal to the distance from the wall at which $\phi = \phi_c$, and the adsorption of the profile, Γ. In the limit that the wetting layer is much thicker than a bulk correlation length,

$$\frac{\Gamma}{\phi_{\text{WL}}-\phi_B}\approx l+l_\Gamma \ , \tag{26}$$

where l_Γ is typically less than 1 nm for the data in this paper. In the same limit, the exponential relaxation of ϕ in the plateau region of the wetting layer results in a disjoining pressure, or equivalently a pressure on the wetting-layer–bulk-liquid interface, of the form [6]

$$\Pi_\xi = Ae^{-l/\xi} \ . \tag{27}$$

In equilibrium and with no other contributions to the disjoining pressure the wetting layer thickness satisfies

$$\Pi_\xi = f_e(\phi_{\text{WL}},\phi_B,t) \ , \tag{28}$$

since in the grand potential f_e is equivalent to the pressure difference between a phase of volume fraction ϕ_B and a phase of volume fraction ϕ_{WL}. We refer to this pressure on the interface as the "bulk correlation force." The numerical solutions of the Euler equation differ by 10% or more from the form in Eq. (27) only for $l < 6$ nm, and in hindsight the simple form for Π_ξ, Eq. (27), suffices for almost all purposes.

For sufficiently thick wetting layers, the long-range dispersion or van der Waals forces on the wetting-layer–bulk-liquid interface will dominate the short-range force characterized by Π_ξ. We describe the dispersion forces using the theory of Dzyaloshinskii, Lifshitz, and Pitaevskii [1], generalized to include effects of the oxide overlayer in the calculation. Simpler theories for dispersion forces do exist, but these theories do not include the retardation effects that can be important for typical layer thicknesses observed in this experiment. Because the resulting formulas have not been published, we give the results in Appendix B. The long-range van der Waals forces between molecules depend on the molecular polarizability of the molecular species and on the distance between molecules. The DLP theory describes the electromagnetic interaction of homogeneous dielectric media, and instead of molecular polarizability requires as parameters the dielectric constant as a function of frequency for each of the media. In practice, the dielectric constant can be adequately modeled by a set of oscillator strengths and oscillator frequencies for each medium, and Appendix B lists these parameters. The Lorentz-Lorenz formula described in Sec. III is used to predict the dielectric constant of liquid mixtures.

Besides assuming that the dielectric layers are considerably thicker than the average molecular spacing, the DLP theory also assumes that the wetting layer and adjacent media are homogeneous and have sharp boundaries, in contrast to the profiles predicted by the free energy of Eq. (18). To estimate the effect of the saturation of ϕ at the surface, we have calculated dispersion forces for the system silicon—1 nm of MC—a layer of M—bulk P and for the same system without the layer of MC. The difference in dispersion forces between the two systems is less than 1% for all wetting layer thicknesses for which the dispersion forces equal or exceed Π_ξ. We conclude that the finite bulk correlation length has little effect on the dispersion forces.

The converse conclusion, that adsorption caused by a finite correlation length varies little with changes in dispersion force, may not be true. Long-range correlations from dispersion forces must lead to a power-law decay of $\phi(z)$ at sufficiently long distances [2,12,13]. The bulk correlation force, Eq. (27), will then become a power law force, $\Pi \sim 1/l^n$, and the results of the free energy assuming only short-range forces, Eq. (19), will be incorrect. We have not attempted to estimate the crossover wetting layer thickness beyond which the power-law form of Π_ξ is valid, but instead look for possible deviations of the experiment from the predictions of the short-range form of Π_ξ.

To predict the adsorption resulting from both dispersion forces and bulk correlation forces, we add the two disjoining pressures linearly. For any adsorption profile calculated from the Euler equation above, we have Γ or l versus $T_\xi - T_{\text{co}}$, where T_ξ is the temperature at which the adsorption was calculated, and T_{co} is the coexistence temperature for a phase of volume fraction ϕ. We can define an effective disjoining pressure by taking Eq. (28) to be valid at all temperatures:

$$\Pi_\xi \equiv f_e(\phi_{\text{WL}},\phi_B,t_\xi) \ , \tag{29}$$

where $t_\xi \equiv (T_\xi - T_c)/T_c$. In the limit $l \gg \xi$, Π_ξ will equal the bulk correlation force on the liquid-liquid meniscus, but for l comparable to the interface width we cannot readily interpret Π_ξ as a force on an interface at some specific distance l from the wall.

We now assume that inclusion of the disjoining pressure resulting from dispersion forces, Π_D, will shift the temperature at which the wetting layer has thickness l, and that this small temperature shift has no appreciable effect on Π_ξ:

$$\Pi_D + \Pi_\xi = f_e(\phi_{\text{WL}},\phi_B,t)$$
$$\approx f_e(\phi_{\text{WL}},\phi_B,t_\xi)+(T-T_\xi)f_e'+O((T-T_\xi)^2) \ , \tag{30}$$

where

$$f_e' \equiv \left[\frac{\partial f_e}{\partial T}\right]_{\phi_{\text{WL}},\phi_B} \ . \tag{31}$$

Only for temperatures within a few millikelvin above coexistence do the dispersion forces contribute significantly to the total disjoining pressure, so evaluating f_e' at coexistence gives a negligible error.

Then for fixed l, dispersion forces shift the temperature away from coexistence to the new value, $T - T_{\text{co}}$:

$$T-T_{\text{co}}\approx(T_\xi-T_{\text{co}})+\frac{\Pi_D}{f_e'} \ . \tag{32}$$

Because we have not altered the ϕ profile, the optical calculations for the ellipsometric parameters δ and ψ do not change with the addition of dispersion forces.

V. OBSERVATIONS

Before the measurements were made, we expected the conceptually simple approach-to-coexistence data to pro-

vide a baseline measurement against which we could compare both the theory and the nonequilibrium data. In practice, the equilibrium measurements in PFMC plus MC proved much more problematic than measurements on another binary liquid system [7].

Over several months at $\approx 45\,°C$ both cells became contaminated with what appeared to be dust or a chemical precipitate. In cell 1 at room temperature, the impurity visibly clustered at the liquid-liquid meniscus, but in cell 2 no impurities were visible with the naked eye. Shortly after filling and at room temperature, liquid completely wet the glass walls and silicon wafer at the solid-liquid-vapor contact line, and M phase completely wet the silicon at the silicon-M-P contact line, for both cells 1 and 2. After several months, cell 1 became incompletely wet at both contact lines at room temperature. Cell 2, in contrast, remained completely wet in both cases throughout the measurements. For these reasons, we believe cell 2 to be superior in cleanliness.

We measured T^* by stirring or shaking the sample and looking for droplets of a second liquid phase suspended in the bulk liquid. In cell 1 the impurities scattered light strongly and as a consequence we could only assign a limit for T^* with the large error bars of ± 30 mK. Within this error, turbidity measurements of a continuously stirred cell gave a T^* in agreement with the visually determined value. To achieve the smaller ± 10-mK errors for cell 2, the approach-to-coexistence data were taken within one month of filling, and only at the end of this period did the impurities interfere with the T^* measurement. Cells 2 and 1 had drift rates for T^* of 1.3 and < 0.5 mK d^{-1}, respectively. Over the one to two day period necessary to perform a full approach-to-coexistence scan, these drift rates give a negligible shift in temperature.

Systematic errors in the data resulting from uncertainties in modeling the oxide and transition layer are not shown in the figures, but are estimated as follows. The in-liquid measurements give values of d_O with considerably more scatter than the in-air measurements, possibly as a result of strain birefringence in the cell walls and the low refractive index mismatch between the liquids and the oxide. The corresponding uncertainty in $\Gamma/(\phi_{WL}-\phi_B)$ is ± 0.4 nm for in-air determinations of d_O and ± 3.5 nm for in-liquid measurements. Variations in the transition layer parameters, within the allowable range determined in Sec. III, give an additional uncertainty of ± 1.0 nm. Both sources of error systematically shift the $\Gamma/(\phi_{WL}-\phi_B)$ versus temperature data with little change in the shape of the curves. For cell 1 we made no in-air measurement of d_O, so the experimental points could have a systematic error of up to 3.5 nm (adding the errors in quadrature). Cell 2, on which we did make in-air measurements, has data with an estimated systematic shift of up to 1.1 nm.

Figure 3 shows the approach-to-coexistence data for cells 1 and 2 along with theoretical estimates of adsorption from Sec. IV. For each data point, we typically waited 3–5 h for thermal equilibration, stirring for ≈ 20 sec 3–4 times over the course of this period, and waiting 30 min after the last stir before making the ellipsometry
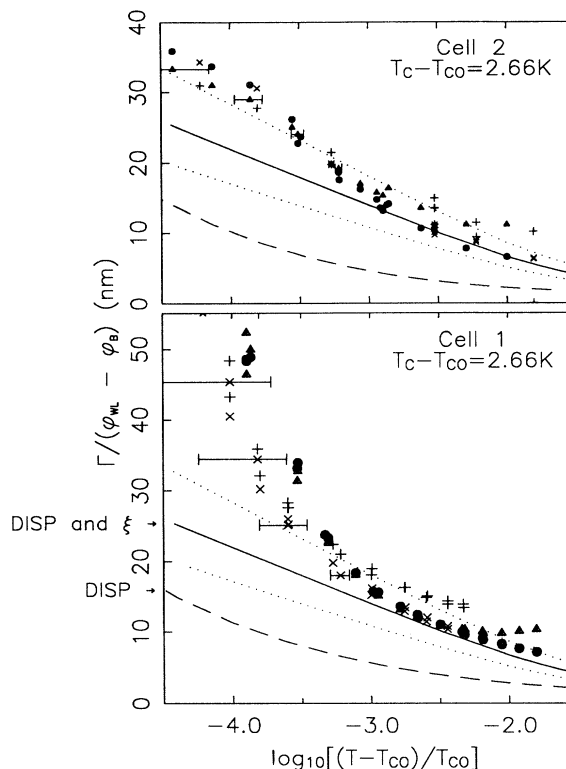
FIG. 3. Approach-to-coexistence data for cells 1 and 2. Triangles and circles refer to adsorption derived from the ellipsometric quantities δ and ψ, respectively. Crosses and plusses also refer to adsorption derived from δ and ψ, but with an order-of-magnitude higher thermal gradient across the cell (see text). For this trajectory, $T_{co}=T^*$. The dashed line labeled DISP shows the adsorption predicted by dispersion force theory alone, and the solid line labeled DISP and ξ shows the adsorption from dispersion forces and bulk correlation forces. Estimated uncertainties in the solid line theory are indicated by the two dotted lines. Scatter in the data is representative of typical errors both in ellipsometry and run to run reproducibility. Horizontal error bars result from uncertainty of T^*.

measurement. Within the limits of the errors, the data of both cells are roughly consistent with the upper limit of the theory of bulk correlation forces and are not consistent with adsorption by dispersion forces alone. The anomalous rise in adsorption at temperatures near T^* observed with cell 1 did not occur in the visibly cleaner cell 2, suggesting that the rise is not an inherent property of the system PFMC plus MC on silicon. As mentioned in Sec. III, we expect the approach-to-coexistence data to depend little on stirring. However, variations in the duration and turbulence of stirring of cell 1, even after thermal equilibrium had been maintained for several hours, gave sizable shifts in $\Gamma/(\phi_{WL}-\phi_B)$. For example, we observed shifts of ± 4 nm at $T-T^*=90$ mK.

To allow comparison with the approach-to-coexistence data, we performed a series of temperature ramp experiments in the two-phase region at a temperature close to T^*. Dropping at least 0.2 K below T^* ensures that a

sufficiently large volume of P phase has been created so that the interface between the bulk P and M phases will extend over the complete cross section of the cell.

As a test of the general solution for $\tilde{\phi}$, Eq. (9), and as a measure of τ_0, we measured the change in adsorption with time following a discontinuous change in ramp rate. Two relaxation runs, with changes in ramp rate of opposite sign, are shown in Fig. 4. Over the range of time studied, the relaxation appears exponential and has a value of τ_0 reproducible to typically 30%. Limits on the curvature of the data indicate that over each decade of variation in $\tilde{\phi}$, τ_0 varies by no more than 40%. From Fig. 4, τ_0 at a stir rate of 1.50 Hz and 3.1 K below T_c is 3.4 h. At 10.5 K below T_c and at the same stir rate, τ_0 drops to 0.44 h. Possibly the larger P volume at the lower temperature exerts more drag than the very small P volume for temperatures just below T^*, resulting in more shear, a smaller L_{DBL}, and a smaller τ_0. Results for both temperatures agree with the order-of-magnitude estimate from Sec. III of 0.75 h. Data at a stir rate of 0.66 Hz were also taken, and by comparing τ_0 for the two stir rates, we can test the prediction from Eq. (12) that $\tau_0 \sim f^{-1/2}$. Averaging the τ_0 ratios from all relaxation runs, we find $\tau_0(1.50$ Hz$)/\tau_0(0.66$ Hz$)=0.69\pm0.20$, in good agreement with the predicted ratio of 0.67. We conclude that the theory for the temperature ramp technique predicts the correct time response of a wetting layer to changes in ramp rate and that the measured characteristic relaxation times agree with theoretical estimates.

With τ_0 known, we can convert the experimental parameter of temperature ramp rate to deviation of temperature from its coexistence value, $T - T_{co}$, or deviation of volume fraction from its coexistence value, $\phi - \phi_{co}$, according to Eq. (10) or Eq. (11). We choose to plot the
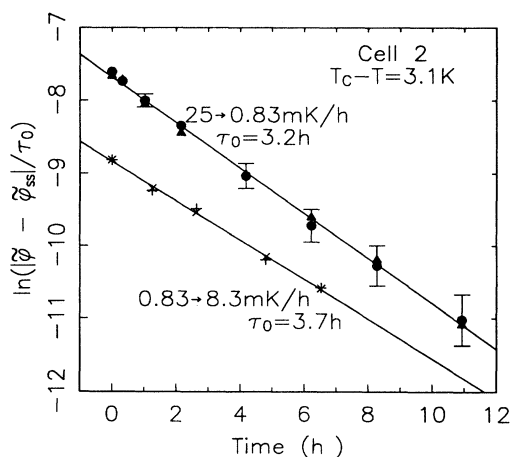
FIG. 4. Relaxation of volume fraction after a change in temperature ramp rate. Fitting the data to a line gives the characteristic relaxation time τ_0 as the negative reciprocal of the slope. Crosses and filled circles represent δ data; plusses and filled triangles represent ψ data. The error bars result from uncertainties in the mapping of the measured ellipsometric parameters to the plotted $\tilde{\phi} - \tilde{\phi}_{ss}$, and the 14% difference in τ_0 for the two relaxations is typical of the run to run reproducibility of τ_0.
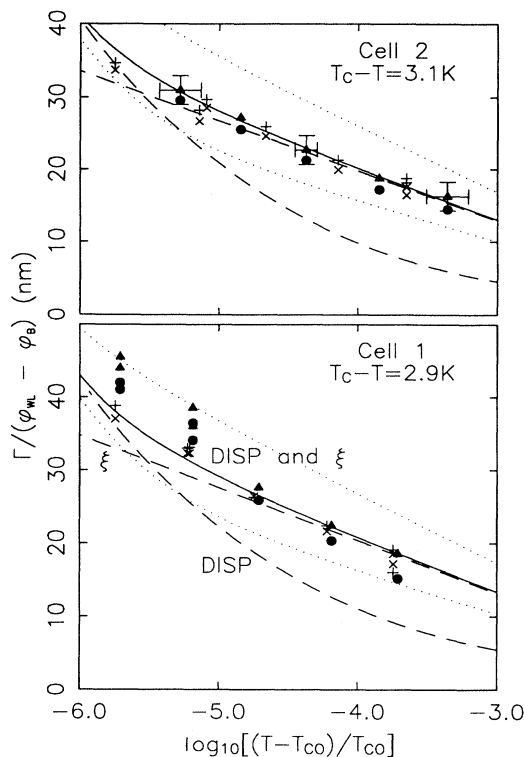
FIG. 5. Temperature ramp data 3 K below T_c. Triangles and circles refer to adsorption derived from the ellipsometric quantities δ and ψ, respectively, for a stir rate of 0.66 Hz. Crosses and plusses also refer to adsorption derived from δ and ψ, but at a stir rate of 1.50 Hz. The dashed line labeled DISP shows the predictions of dispersion force theory alone, the dashed line labeled ξ shows the predictions of the bulk correlation force, and the solid line corresponds to the sum of dispersion and correlation forces. Estimated uncertainties in the solid line theory are indicated by the two dotted lines. Errors in the ellipsometric parameters and in τ_0 give the error bars shown.

steady state ramp data as normalized adsorption versus $T - T_{co}$ to allow easy comparison with the approach-to-coexistence data.

Figure 5 shows the steady state ramp data for cells 1 and 2 at a temperature close to T^*. The data of cell 1 display more scatter than the cell 2 data, but the two data sets agree with one another and also agree with the theory of adsorption that assumes short-range, exponential decay of correlations. The data do not conclusively distinguish between the theory with or without dispersion forces, because at this temperature and for the experimentally accessible range of $T - T_{co}$, dispersion forces are weak relative to bulk correlation forces. A stir rate of 1.50 Hz and a ramp rate of 0.25 mK h^{-1}, the slowest used for these experiments, give a deviation from coexistence of $T - T_{co} = 0.60\pm0.25$ mK, a resolution 40$\times$ superior to the cell 2 approach-to-coexistence data. Note that if the worst case T^* drift, 1.3 mK d^{-1}, reflects a uniform upwards shift of the whole coexistence curve at the same rate, then this drift is equivalent to a negative ramp

rate of 60 μK h^{-1}, a 24% shift in the effective $\dot{T}$. This effect and the thermal stability of the thermostat set a practical lower limit for $T - T_{\mathrm{co}}$. Measurements of the adsorption in cell 1 at distances of 1.6, 4.0, and 7.2 mm below the liquid-liquid meniscus gave results independent of height to within the estimated error, as expected for a continuously stirred system with minimal gravitational sedimentation. For comparison, we have calculated the gradient in ϕ resulting from gravity in an unstirred cell with no temperature drift [36], $\nabla\phi = g(\rho_{\mathrm{PFMC}} - \rho_{MC})(\partial\phi/\partial\Delta)$. At $T_c - T = 3.0$ K and a distance of 1 cm below the meniscus, the shift from coexistence is equivalent to $(T - T_{\mathrm{co}})/T_{\mathrm{co}} = 1.7 \times 10^{-5}$.

Independent of the uncertainty in oxide and transition layer modeling, the cell 2 ramp data and cell 2 approach-to-coexistence data differ by an amount somewhat larger than the estimated uncertainty in the data, even though both sets of data lie within the bounds of the theoretical curves. We do not know if this represents a physical effect or an underestimate of the error in one or both measurements.

At temperatures significantly lower than T^*, dispersion forces become more important as the bulk correlation length drops in magnitude. We made a series of ramp measurements at 10.5 K below T_c with the intention of searching for stronger dispersion force affects. As seen in Fig. 6, at this temperature the ramp data map out the crossover from adsorption dominated by bulk correlation forces to adsorption dominated by dispersion forces. At the lowest values of $T - T_{\mathrm{co}}$, the data agree with the DLP theory, and at higher deviations from coexistence the data are consistent with the simple superposition of forces outlined in Sec. IV.

We performed a variety of control experiments to confirm that the above results are not significantly perturbed by imperfect temperature control. Using heaters embedded into either the top or bottom of the innermost thermostat shell, we artificially induced thermal gradients

of approximately twice the measured limit, described in Sec. II. Ramp data taken with the top heater on and with the bottom heater on had differences in wetting layer thickness of less than 0.1 nm. When we increased the laser power by a factor of 10 while ramping at the slowest-rate, the wetting layer thickness changed by less than 1 nm, evidence that laser heating is not important. We made no direct measurements of thermal gradients while taking the approach-to-coexistence data, but we do note that strongly increasing the thermostat thermal gradients by removing the stage-1 thermostat shell and increasing the stage-3 heater output by approximately a factor of 10 gave no noticeable change in adsorption. We estimate that the thermal gradients are 0.1 mK cm^{-1} with the stage-1 shell, and 1 mK cm^{-1} without the shell. To confirm that the stirring used for the ramp technique did not cause a shear instability at the wetting-layer–bulk-liquid interface, we measured the adsorption with the stirrer on and then remeasured the adsorption after five minutes of no stirring. We observed less than 0.1 nm change in wetting layer thickness between the measurements.

VI. DISCUSSION

The reproducibility of the temperature ramp data, its agreement with reasonable theoretical predictions, the observed exponential relaxations of volume fraction, and measured values of τ_0 close to the estimated value all suggest that the theory for the temperature ramp technique outlined in Sec. III is correct.

For the data at $T_c - T = 3$ K, the crossover between a disjoining pressure dominated by dispersion forces and disjoining pressure dominated by bulk correlation forces occurs at $l \approx 30$ nm. The correlation length at this temperature is 3.0 nm, so the agreement between the measurements and the theory implies that the exponential relaxation of ϕ dominates any power-law relaxation out to at least five correlation lengths. Consequently, we have no evidence that the simple Widom theory inadequately describes the bulk correlation force.

The agreement between the ramp data and the theory for bulk correlation forces may be somewhat fortuitous, since at large l capillary waves contribute a term to Π of the form $A \exp(-l/\xi)$, the same functional form found with a bulk correlation force [5]. Although both theory and experiment have fairly large systematic errors in l or $\Gamma/(\phi_{\mathrm{WL}} - \phi_B)$, based on the quantitative agreement between the experimentally measured and theoretically predicted adsorption we can conclude that capillary waves contribute a disjoining pressure that is of the same order of magnitude as or less than the disjoining pressure resulting from bulk correlations.

The theory for $T_c - T = 10.5$ K indicates a strong contribution to the disjoining pressure by dispersion forces. The agreement between this theory and the cell 2 ramp data confirms the validity of the DLP theory for calculations of forces for liquid mixtures in a solid-liquid-liquid configuration, complementing previous experiments on forces in systems with a solid-liquid-vapor, solid-vapor-solid, or solid-liquid-solid geometry [37–39].

We have already mentioned that the observed impuri-
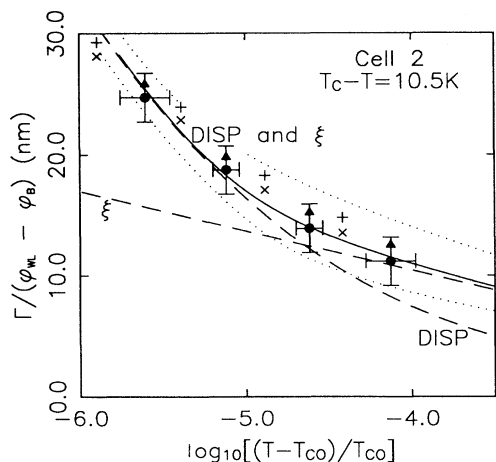
FIG. 6. Temperature ramp data 10.5 K below T_c. The code for the symbols and lines is identical to the code for Fig. 5.

ties hindered the measurement of T^*, especially in cell 1, and that this difficulty contributes large errors to the approach-to-coexistence data. For the earliest determinations of T^* for cell 2 we saw no impurities, however, and yet the cell 2 approach-to-coexistence data do differ somewhat from the ramp data for similar $T - T_{co}$. Two possible experimental difficulties that would affect the equilibrium data but not the temperature ramp data independent of any uncertainty in T^* follow.

1. If the free energy of an impurity particle is reduced by being surrounded by M liquid or by being localized at a liquid-liquid meniscus, the creation of a thick wetting layer even in the single-phase region would provide an energetically favorable site for the impurities. In the two-phase region, the impurities could accumulate at the bulk liquid-liquid meniscus or in the bulk M phase, and the adsorption would be less than in the single-phase region.

2. If M liquid adsorbs on large surface area impurities or condenses inside small crevices of the sample cell, and if the quantity of adsorption increases as the temperature approaches two-phase coexistence, the approach-to-coexistence trajectory will bend towards smaller ϕ values just above the coexistence curve. The distorted trajectory will result in a distorted plot of $\Gamma/(\phi_{WL} - \phi_B)$ versus $(T - T_{co})/T_{co}$. If an identical loss of MC occurs in the two-phase region, the only effect will be a negligible change in the volumes of the two coexisting phases, with a correspondingly negligible change in τ_0.

In a previous study of the effects of stirring on wetting layers [40], the early stage growth of the layers occurred over periods on the order of one hour for stir rates close to 1 Hz, in disagreement with a theory describing diffusion in the vicinity of the wetting layer [8]. We now believe that the initial jump up in temperature, used to reduce the wetting layer thickness, leaves the bulk liquid phase far in the single-phase region and that diffusion limited transport across the liquid-liquid meniscus governs the relaxation of the concentration back to its steady state value. The characteristic time for such a process is τ_0, which has a typical magnitude in qualitative agreement with the observed growth times.

Many of the characteristics of the temperature ramp technique make it an ideal tool for exploring the thermodynamics and adsorption properties near wetting transitions. With equilibration times of a few hours, the technique can reliably probe states in the range 50–0.5 mK above the coexistence curve and is not confined to a single cell concentration per cell, unlike the approach-to-coexistence method. Furthermore, thermally induced convection [10,11,36] does not disturb the steady state, which is not true when gravity is used to push the system off coexistence. As an example of a potential application, the temperature ramp technique could be used to search for the line of prewetting transitions predicted to exist for any wetting system with a first-order wetting transition [41,42]. A previous search which gave null results could only reliably measure adsorption states more than 50 mK above coexistence [21], a sensitivity roughly two orders of magnitude worse than the sensitivity potentially possible with the ramp technique.

APPENDIX A: DATA MAPPINGS

As explained in Sec. II, we combine the theoretical adsorption profiles with optical models to obtain a map between $\Gamma/(\phi_{WL} - \phi_B)$ and δ and ψ. To allow conversion of the data points back to the original δ and ψ values, Table I lists for the cell 2 figures the polynomial coefficients of the expressions

$$\frac{\Gamma}{\phi_{WL} - \phi_B} = \sum_{i=0}^{3} A_i x^i \tag{A1}$$

where x may stand for either δ or ψ. The incident angle was 69°, and the mapping assumes a transition layer thickness of 0.7 nm, a transition layer refractive index of 3.2, and an oxide thickness from in-air measurements of 1.52 nm.

APPENDIX B: DISPERSION FORCE THEORY

In this appendix we present the formulas necessary to extend the dispersion force theory developed by Dzy-

TABLE I. Coefficients for map of adsorption to ellipsometric parameters. The units for $\Gamma/(\phi_{WL} - \phi_B)$ are nanometers, and radians for δ and ψ.

Fig.	x	A_0	A_1	A_2	A_3
3	δ	2.04078×10^3	-2.03540×10^3	6.92846×10^2	-8.04580×10^1
3	ψ	-4.39886×10^2	1.35211×10^4	-1.36705×10^5	4.92549×10^5
5	δ	4.87552×10^3	-5.44344×10^3	2.05579×10^3	-2.61846×10^2
5	ψ	-2.83970×10^2	7.91492×10^3	-7.02146×10^4	2.30116×10^5
6	δ	1.73981×10^3	-1.82854×10^3	6.57137×10^2	-8.04870×10^1
6	ψ	-2.44217×10^2	6.59126×10^3	-5.72394×10^5	1.81738×10^5

aloshinskii, Lifshitz, and Pitaevskii [1] (DLP) to the case of four homogeneous, planar dielectric media. Sandwiched between the semi-infinite media 1 and 4 are medium 2 adjacent to medium 1 and of fixed thickness l_2, and medium 3 of thickness l_3, across which the force is calculated. The DLP paper develops a general theory for the dispersion forces in isotropic but inhomogeneous dielectric media. To actually calculate a force requires first finding a Green function appropriate to the system, and simple planar geometries facilitate this task.

For the case of a homogeneous dielectric medium, the Green function consists of simple and analytic exponential terms. The Green function for a dielectric slab between two semi-finite dielectric media can be found by matching the Green functions for each medium, subject to appropriate boundary conditions, and DLP give the final result for this geometry in Eq. 4.13 (DLP). Subsequent formulas in the DLP paper make various approxi-

mations, many of which can introduce large errors unless carefully applied. Since Eq. 4.13 (DLP) can be readily evaluated by a computer, there is little point in using the approximations.

The Green function for the four-media case follows the derivation for the three-media case with the addition of one more plane at which boundary conditions are matched. With the two exceptions of using l_i for the thickness of medium i and denoting the disjoining pressure by Π_D instead of $-F$, we adopt the notation of DLP and will not define each variable. In particular, Δ refers not to a free-energy amplitude but to a parameter in the DLP theory. We can rewrite Eq. 4.13 (DLP) as

$$\Pi_D(l_3) = \frac{k_B T}{\pi c^3} \sum_{n=0}^{\infty} {}' (\epsilon_3)^{3/2} \xi_n^3 \int_1^{\infty} dp\, p^2 \left[\frac{1}{\Delta} + \frac{1}{\bar{\Delta}} \right], \quad \text{(B1)}$$

with

$$\Delta = 1 - \left[\frac{w_3 + w_4}{w_3 - w_4} \right] \exp(2w_3 l_3) \left[\frac{(w_3 + w_2)(w_1 + w_2)\exp(2w_2 l_2) + (w_3 - w_2)(w_2 - w_1)}{(w_3 - w_2)(w_1 + w_2)\exp(2w_2 l_2) + (w_3 + w_2)(w_2 - w_1)} \right], \quad \text{(B2)}$$

$$w_i = \frac{\xi_n}{c} [\epsilon_i + \epsilon_3(p^2 - 1)]^{1/2}, \quad \text{(B3)}$$

and $\bar{\Delta}$ obtained by replacing w_i by ϵ_i/w_i, except in the exponents. When the dielectric properties of medium 2 approach the dielectric properties of medium 1, the formula for Δ approaches the three-media result of DLP.

For ease of numerical computation, we transform Eq. (B1) using $u = 1/p$ to get for the contribution of the nonzero frequencies

$$\Pi_{NZ}(l_3) = \frac{k_B T}{\pi c^3} \sum_{n=1}^{\infty} (\epsilon_3)^{3/2} \xi_n^3 \int_0^1 \frac{du}{u^4} \left[\frac{1}{\Delta} + \frac{1}{\bar{\Delta}} \right]. \quad \text{(B4)}$$

In the special $n = 0$ case, we use the transformation $u/(1-u) = Kp$, $K \equiv (\xi_0 l_3/c)(\epsilon_{30})^{1/2}$, where ϵ_{30} is the zero-frequency dielectric constant of medium 3. The result is

$$\Pi_Z(l_3) = \frac{k_B T}{2\pi(l_3)^3} \int_0^1 du \frac{u^2}{(1-u)^4 \bar{\Delta}} \quad \text{(B5)}$$

with

$$\bar{\Delta} = 1 - \left[\frac{\epsilon_{30} + \epsilon_{40}}{\epsilon_{30} - \epsilon_{40}} \right] \exp\left[\frac{2u}{1-u} \right] \left[\frac{(\epsilon_{30} + \epsilon_{20})(\epsilon_{10} + \epsilon_{20})\exp[2l_2 u/l_3(1-u)] + (\epsilon_{30} - \epsilon_{20})(\epsilon_{20} - \epsilon_{10})}{(\epsilon_{30} - \epsilon_{20})(\epsilon_{10} + \epsilon_{20})\exp[2l_2 u/l_3(1-u)] + (\epsilon_{30} + \epsilon_{20})(\epsilon_{20} - \epsilon_{10})} \right]. \quad \text{(B6)}$$

TABLE II. Dielectric parameters for Si, SiO_2, C_7F_{14}, and C_7H_{14}. Each material is assigned an oscillator frequency in the infrared, ω_{ir}, and in the ultraviolet, ω_{uv}. The constants ϵ_{fir} and ϵ_{vis} are approximately equal to the dielectric constant in the far-infrared and visible regions of the spectrum, far away from either oscillator frequency.

Material	ϵ_{fir}	ϵ_{vis}	ω_{ir} $(10^{15} \text{ rad sec}^{-1})$	ω_{uv} $(10^{15} \text{ rad sec}^{-1})$
Si	11.8	11.8	0.188	20.33
SiO_2	3.81	2.10	0.24	26.0
C_7F_{14}	1.82	1.634	0.24	18.0
	1.82	1.636	0.24	26.0
C_7H_{14}	2.020	1.994	0.55	18.3

To apply these equations to PFMC plus MC mixtures against silicon, we adopt the dielectric models as explained by Hough and White [43] and as applied to a binary liquid system by Kayser [44]. We replace the spectrum of electromagnetic absorption bands in each medium by two single frequency oscillators, one in the infrared and one in the ultraviolet. The resulting dielectric constant as a function of imaginary frequency is

$$\epsilon(i\xi) = \frac{\epsilon_{fir} - \epsilon_{vis}}{1 + (\xi/\omega_{ir})^2} + \frac{\epsilon_{vis} - 1}{1 + (\xi/\omega_{uv})^2} + 1 \ . \qquad (B7)$$

We use literature data on dielectric constants [45,46], refractive indices [23,24], and optical-absorption spectroscopy [47] to find the frequencies and oscillator strengths of the model, listed in Table II.

The predominant error in the parameters is the PFMC ultraviolet absorption pole frequency. We determine this frequency by fitting visible and near-uv refractive index data to a single pole oscillator model, but the fit is much poorer than for other typical liquids or solids. Because MgF_2 refractive index data also cannot be fit well with a single oscillator, we suspect that the poor fit is charac-

teristic of fluorine compounds and not a result of poor PFMC data. We have listed two plausible oscillator models in the table. As an example, at 10.5 K below the critical temperature and for wetting layer thicknesses between 14 and 34 nm, the model with the higher oscillator frequency gives Π_D 20–10 % lower than the lower-frequency model.

The electrical conductivity σ of the silicon causes a divergence in the dielectric constant at zero frequency, and although the magnitude of the effect will be orders of magnitude smaller than in a metal, this will in principle modify the disjoining pressure. We estimate the magnitude of this effect by letting the zero-frequency dielectric constant of silicon go to infinity for the zero-frequency term, and for the nonzero frequencies adding a term $4\pi\sigma/\xi$ (cgs units) to the dielectric constant for silicon [48]. Because the dielectric constant diverges only in the long-wavelength limit and the dispersion force integral depends on a range of wave vectors, this approximation of the dielectric constant overestimates the effect. The difference between Π_D with and without the correction is less than 1% for wetting layer thicknesses less than 60 nm, which is negligible.

---

*Present address: National Institute of Standards and Technology, Gaithersburg, MD 20899.

[1] I. E. Dzyaloshinskii, E. M. Lifshitz, and L. P. Pitaevskii, Adv. Phys. 10, 165 (1961).

[2] P. G. de Gennes, J. Phys. (Paris) Lett. 42, L377 (1981).

[3] Dean Ripple, Xiao-lun Wu, and Carl Franck, Phys. Rev. B 38, 9054 (1988).

[4] R. F. Kayser, Phys. Rev. Lett. 56, 1831 (1986); J. Phys. (Paris) 49, 149 (1988).

[5] Michael E. Fisher, J. Chem. Soc. Faraday Trans. 2 82, 1569 (1986).

[6] B. Widom, in Phase Transitions and Critical Phenomena 2, edited by C. Domb and M. Green (Academic, New York, 1972), Chap. 3; J. Chem. Phys. 68, 3878 (1978); Michael E. Fisher and Pierre-Gilles de Gennes, C. R. Acad. Sci. (Paris), Ser. B 287, 207 (1978); Andrea J. Liu and Michael E. Fisher, Phys. Rev. A 40, 7202 (1989).

[7] Xiao-lun Wu, Mark Schlossman, and Carl Franck, Phys. Rev. B 33, 402 (1986).

[8] R. F. Kayser, M. R. Moldover, and J. W. Schmidt, J. Chem. Soc. Faraday Trans. 2 82, 1701 (1986).

[9] M. Giglio and A. Vendramini, Phys. Rev. Lett. 35, 168 (1975).

[10] G. K. Batchelor, Q. Appl. Math. XII, 209 (1954).

[11] J. E. Hart, J. Fluid Mech. 49, 279 (1971).

[12] S. Dietrich (unpublished).

[13] S. Dietrich and M. Napiórkowski, Phys. Rev. A 43, 1861 (1991).

[14] Douglas J. Durian and Carl Franck, Phys. Rev. A 40, 5220 (1989).

[15] Dean Ripple, Physics Ph.D. thesis, Cornell University, 1991, Chap. 4. (University Microfilms International, Ann Arbor, MI).

[16] R. J. Archer, Manual on Ellipsometry (Gaertner Scientific, Chicago, 1968).

[17] R. M. Azzam and N. M. Bashara, Ellipsometry and Polar-

ized Light (North-Holland, New York, 1977).

[18] D. Scott Becker, William R. Schmidt, Charlie A. Peterson, and Don C. Burkman, Microelectronics Processing, edited by Lawrence A. Casper (American Chemical Society, Washington, DC, 1986), p. 366.

[19] PFMC was 97% pure, from Pflatz and Bauer, Waterbury, CT; MC was 99+% pure, stock item 30,030-6 from Aldrich Chemical, Milwaukee, WI. The silicon was p-doped monitor grade, with a (100) surface.

[20] R. B. Heady and J. W. Cahn, J. Chem. Phys. 58, 896 (1973).

[21] James W. Schmidt and Michael R. Moldover, J. Chem. Phys. 84, 4563 (1986).

[22] S. R. de Groot and P. Mazur, Non-Equilibrium Thermodynamics (Dover, New York, 1984), p. 244.

[23] J. P. Wibaut, H. Hoog, S. L. Langedijk, J. Overhoff, and J. Smittenberg, Rec. Trav. Chim. Pays-Bas 58, 329 (1939).

[24] E. F. Yamshchikov, Opt. Spektrosk. 12, 798 (1962) [Opt. Spectrosc. (USSR) 12, 452 (1962)].

[25] Max Born and Emil Wolf, Principles of Optics, 6th ed. (Pergamon, Oxford, 1980), p. 85.

[26] D. E. Aspnes and J. B. Theeten, J. Electrochem. Soc. 127, 1359 (1980).

[27] Rolf Hulthén, Phys. Scr. 12, 342 (1975).

[28] Max Born and Emil Wolf, Ref. [25], p. 51 and following.

[29] E. M. Lifshitz and L. P. Pitaevskii, Statistical Physics, Part 1, 3rd ed. (Pergamon, Oxford, 1980), p. 471.

[30] J. S. Rowlinson and B. Widom, Molecular Theory of Capillarity (Clarendon, Oxford, 1982), Chaps. 3 and 9.

[31] John W. Cahn, J. Chem. Phys. 66, 3667 (1977).

[32] M. R. Moldover, Phys. Rev. A 31, 1022 (1985).

[33] B. E. Sundquist and R. A. Oriani, J. Chem. Phys. 36, 2604 (1962).

[34] M. Vicentini-Missoni, J. M. H. Levelt Sengers, and M. S. Green, J. Res. Natl. Bur. Stand. Sect. A 73, 563 (1969).

[35] A. Kumar, H. R. Krishnamurthy, and E. S. R. Gopal,

Phys. Rep. **98**, 57 (1983).

[36] Dean Ripple, Ref. [15], Chap. 5.

[37] E. S. Sabisky and C. H. Anderson, Phys. Rev. A **7**, 790 (1973).

[38] J. N. Israelachvili and D. Tabor, Proc. R. Soc. London, Ser. A **331**, 19 (1972).

[39] B. V. Derjaguin, Y. I. Rabinovich, and N. V. Churaev, Nature (London) **272**, 313 (1978).

[40] Xiao-lun Wu, Dean Ripple, and Carl Franck, Phys. Rev. A **36**, 3975 (1987).

[41] E. H. Hauge and M. Schick, Phys. Rev. B **27**, 4288 (1983).

[42] Asok K. Sen and C. Ebner, Phys. Rev. B **33**, 5076 (1986).

[43] David B. Hough and Lee R. White, Adv. Colloid Interface Sci. **14**, 3 (1980).

[44] R. F. Kayser, Phys. Rev. B **34**, 3254 (1986).

[45] F. H. Müller, in *Table of Dielectric Constants of Pure Liquids,* edited by Arthur A. Maryott and Edgar R. Smith, Natl. Bur. Stand. (U.S.) Circular No. 514 (U.S. GPO, Washington, DC, 1951).

[46] D. W. Cottrell, in *Conference on Dielectric Materials, Measurements and Applications* (Institution of Electrical Engineers, London, 1970), p. 322.

[47] *Selected Infrared Spectral Data,* Thermodynamics Research Center Hydrocarbon Project, edited by Beverly Boyd (Texas A&M University, College Station, TX, 1983), spectra 0996, 1139, and 1140.

[48] J. D. Jackson, *Classical Electrodynamics,* 2nd ed. (Wiley, New York, 1975), p. 287.